analytical chemistry

pubs.acs.org/ac Article

PDMS Curing Inhibition on 3D-Printed Molds: Why? Also, How to Avoid It?

Bastien Venzac,* Shanliang Deng, Ziad Mahmoud, Aufried Lenferink, Aurélie Costa, Fabrice Bray, Cees Otto, Christian Rolando, and Séverine Le Gac*

Cite This: *Anal. Chem.* 2021, 93, 7180–7187 Read Online

ACCESS | Metrics & More | Article Recommendations | Supporting Information

ABSTRACT: Three-dimensional (3D)-printing techniques such as stereolithography (SLA) are currently gaining momentum for the production of miniaturized analytical devices and molds for soft lithography. However, most commercially available SLA resins inhibit polydimethylsiloxane (PDMS) curing, impeding reliable replication of the 3D-printed structures in this elastomeric material. Here, we report a systematic study, using 16 commercial resins, to identify a fast and straightforward treatment of 3D-printed structures and to support accurate PDMS replication using UV and/or thermal post-curing. In-depth analysis using Raman spectroscopy, nuclear magnetic resonance, and high-resolution mass spectrometry revealed that phosphine oxide-based photo-initiators, leaching out of the 3D-printed structures, are poisoning the Pt-based PDMS catalyst. Yet, upon UV and/or thermal treatments, photo-initiators were both eliminated and recombined into high molecular weight species that were sequestered in the molds.

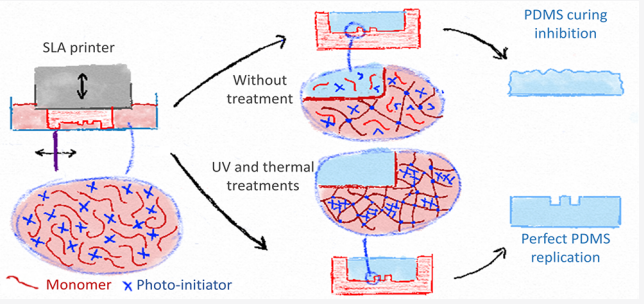

The introduction of soft lithography has greatly contributed to the expansion of the field of microfluidics into nonspecialized laboratories.[1,2] In this technique, structures on a mold are replicated into a transparent, nonfragile, and elastomeric material, polydimethylsiloxane (PDMS), using standard laboratory equipment. PDMS remains the number-one material to produce miniaturized (bio)-analytical devices for molecular separation, biosensing, diagnostic purposes, cell separation, single cell and extracellular vesicle analysis, droplet microfluidics, and for creating mini-organ models *in vitro*.[3]

Molds for soft lithography have historically been produced using the standard clean-room processes of photolithography and silicon dry-etching,[1] which ensure high replication accuracy and high resolution in the low micrometer range. Yet, these techniques are expensive and time-consuming; and they request access to dedicated facilities and extensive training. Alternative technologies have been explored to produce molds, while addressing these issues. For example, micromachining of aluminum, brass, or poly(methyl methacrylate) plates using micromilling allowed for the creation of nonplanar geometries in about 2 h, with excellent replication of channel down to 10 μm in size.[4] Additive approaches have also been proposed using wax printers,[5] laser printers,[6] fused-deposition modeling,[7] or multijet three-dimensional (3D) printers.[8] Yet, these techniques all exhibit a lower resolution and often yield rough surfaces, which is far from being ideal for casting. Using stereolithography (SLA), 3D structures are created through the layer-by-layer polymerization of a photosensitive resin in a tank using UV light, for example, at 405 nm, by scanning a laser beam in a plane or projecting images for each plane using digital micromirrors or liquid-crystal display screens.[9] The SLA lateral resolution ranges from 50 μm for printers costing less than $1000, down to <5 μm for more advanced setups.[10] While SLA has been widely used to produce molds for PDMS casting,[11−16] PDMS curing is inhibited in the vicinity of these 3D-printed molds, for nearly all commercially available SLA resins, precluding faithful replication. Alternatively, PDMS strongly adheres to those molds.[12,16,17] Therefore, SLA molds must be treated, with, for example, UV post-curing,[11−16,18,19] temperature,[12,14,17−19] solvents,[11,13,16] sonication,[11] silanization,[12,16,17] or a coating[11,20] (for an overview, see Supporting Information Table S1). However, all these treatments have been reported for one specific resin.

The Pt-based catalyst found in PDMS (Sylgard 184) cross-links vinyl-terminated oligomers via a hydrosilylation mechanism.[21] Tri-organophosphite, vinyl, maleate, fumarate, and β-alkynol can reversibly or irreversibly inhibit PDMS curing due to their strong affinity for the catalyst or by sequestering it in small droplets.[22−24] Moreover, 3D-printed objects release a variety of chemicals in solution, including polyethylene glycols,

Received: November 24, 2020
Accepted: April 23, 2021
Published: May 7, 2021

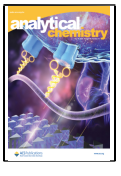

https://doi.org/10.1021/acs.analchem.0c04944
Anal. Chem. 2021, 93, 7180−7187

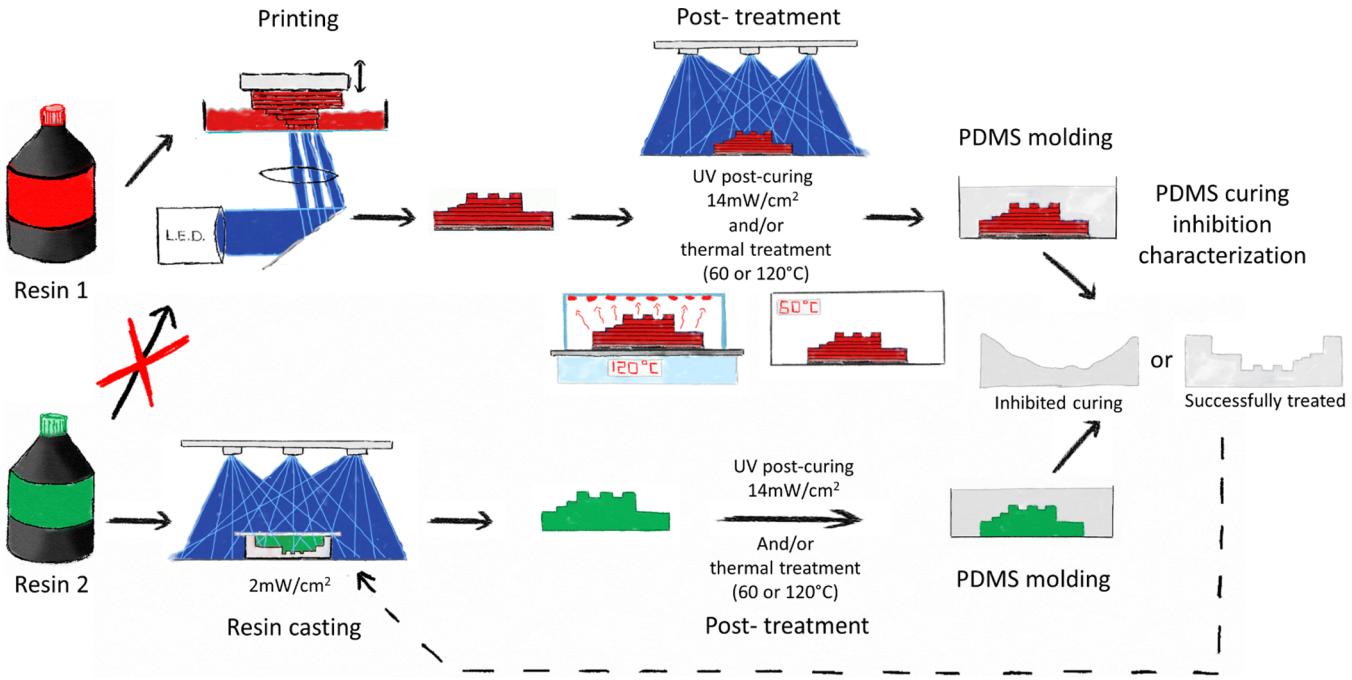

Figure 1. Schematic overview of the experimental approach. A test mold fabricated in resin 1 (FTD deep black or industrial red) was exposed to UV and/or heat, and its PDMS curing inhibition was evaluated (see Figure 2). The resulting PDMS layer was used to cast molds from other resins (resin 2, here) not processable using our printer. These molds were exposed to UV and/or heat, and their PDMS curing inhibition was characterized.

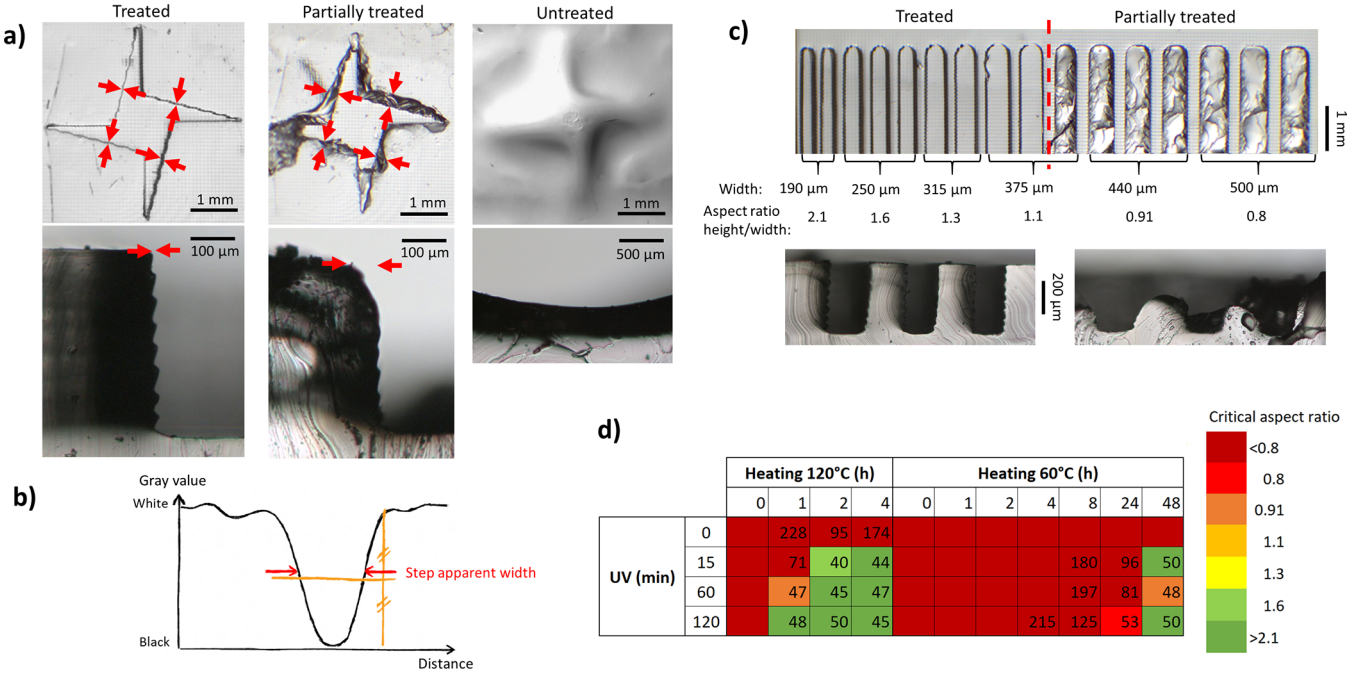

Figure 2. (a) Microscopy picture of shuriken structures in PDMS for three representative conditions (from left to right; successful, partial replication, and no treatment. Top: top view of PDMS replicates; bottom: cross-sections of PDMS replicates). Red arrows indicate the location of the measurements. (b) Typical gray value profile recorded along the red arrows in (b) to determine the apparent step width. (c) Microscopy pictures of the comb structures in PDMS after successful (left) and partial post-treatment (right), top view (top), and cross-section (bottom). (d) Example of post-treatment screening for FTD industrial red. Numbers correspond to the *apparent step width* (no value provided in the case of serious PDMS curing inhibition) and the colors to the *critical aspect ratio* (as detailed in the Experimental Section).

diethyl-phthalates,[25] unreacted monomers,[26] and phosphine-oxide photoinitiators,[27] which can also inhibit the catalyst. However, to the best of our knowledge, PDMS curing inhibition has never been investigated in the case of 3D-printed molds, and no study has examined the role of post-treatments.

Here, we first developed a generic post-treatment recipe for molds produced from 16 commercial SLA resins. PDMS curing inhibition on those molds was systematically quantified, and the influence of a UV and/or heat treatment was evaluated. Using Raman spectroscopy, nuclear magnetic resonance (NMR), and

https://doi.org/10.1021/acs.analchem.0c04944
Anal. Chem. 2021, 93, 7180−7187

Table 1. Post-Treatments Established for 3D-Printed Molds as Determined in This Study for 16 Commercial Resins[a]

			recipe 1		recipe 2	
company/provider	resin name	resin characteristics	UV	heating (120 °C)	UV	heating (60 °C)
Fun-To-Do	standard black		1 h	4 h	X	X
	standard red		2 h	8 h	X	X
	industrial black	composite	15 min	2 h	X	X
	industrial red	composite	15 min	2 h	15 min	48 h
	deep black	composite (carbon nanotube)	15 min	2 h	1 h	48 h
Formlabs	black		0 h	1 h	0 h	24 h
	flex	flexible	0 h	2 h	2 h	0 h
	HT	high temperature	0 h	1 h	0 h	1 h
	clear	transparent	0 h	1 h	0 h	24 h
Envisiontec	PIC100	casting resin	2 h	4 h	X	X
	E-shell 300	transparent, biocompatible	0 h	1 h	0 h	24 h
	R11		2 h	4 h	X	X
DWS	DL260	composite with ceramic	0 h	1 h	2 h	24 h
	DS3000	transparent, biocompatible	0 h	2 h	0 h	24 h
	GL4000	flexible	1 h	8 h	4 h	0 h
	GM08	flexible, transparent	1 h	8 h	2 h	24 h

[a]"X" stands for the absence of treatment found in the range of tested duration of the two steps.

high-resolution mass spectrometry (HR-MS), we next elucidated this curing inhibition mechanism and examined how the proposed post-treatment remedied to this issue.

MATERIALS AND METHODS

Experimental Approach for Identifying Post-Treatment Recipes for 16 Commercial Resins. First, 3D-printed molds were treated with UV and heat (60 or 120 °C) before PDMS casting. Curing inhibition was assessed using two test structures through image analysis. To extend the scope of our study to a wider range of resins that could not be processed with our printer, we cast and UV-cured other resins on PDMS molds presenting the same test structures (Figure 1).

Mold 3D-Printing. Molds were printed using a digital light processing printer (FlashForge Hunter, FlashForge, Jinhua City, China), with a 405 nm light-emitting diode (LED) source, a pixel size of 62.5 × 62.5 μm^2, and a step height of 50 μm using industrial red and deep black resins (Fun-To-Do, Alkmaar, The Netherlands). Molds were rinsed with isopropanol before treatment.

Mold Treatment. Printed molds were post-cured in a homemade 405 nm LED UV box for 15 min, 1, 2, or 4 h at 14 mW/cm^2 and/or exposed to a thermal treatment at either 60 °C (in an oven) for 1, 2, 4, 8, 24, or 48 h or at 120 °C (on a hotplate covered with a glass dish) for 1, 2, 4, or 8 h.

Quantitative Evaluation of the PDMS Curing Inhibition. A 1:10 w/w ratio of the curing agent and PDMS prepolymer (Sylgard 184, Dow Corning, USA) was mixed, degassed under vacuum, and poured on the molds. PDMS was cured for 3 h at 60 °C. Top pictures of the PDMS replicas were captured with a binocular microscope equipped with a camera (Motic sMZ-171, Motic, Xiamen, China) using backlight illumination. PDMS inhibition was quantified using two 400 μm high test structures, a shuriken (Figure 2a), and a comb (Figure 2c), comprising a series of 2 mm long teeth with widths of 190−500 μm (aspect ratio height/width of 2.1−0.8). The width of the transition between the bottom and the top of the shuriken was measured at four locations using ImageJ (NIH, Bethesda, USA), as depicted in Figure 2a. The width at half maximum of the peak corresponding to the transition on a gray-value plot, orthogonal to the wall, was determined (Figure 2b), and these four values were averaged into a so-called "*apparent step width*" (in μm). From the thinnest perfectly replicated structure in the comb, a "*critical aspect ratio*" was extracted.

SLA Resin Mold Casting. PDMS replicates from printed molds, after post-treatment, were exposed to plasma (Cuter, Femto Science, Gyeonggi-Do, South Korea) for 40 s at 50 W, 50 kHz, and 0.7 mbar and silanized by vapor deposition of (1*H*,1*H*,2*H*,2*H*-perfluorooctyl)-trichlorosilane for 20 min in a closed container. 16 resins were cast on these PDMS countermolds: Fun-To-Do industrial black and red, standard black, standard red, and deep black; Formlabs black, clear, flex, and high temperature (Formlabs, Sommerville, USA); DWS GL4000, GM08, DS3000, and DL260 (DWS, Thiene, Italy); EnvisionTec PIC100, R11, and E-Shell 300 (EnvisionTec, Dearborn, USA). Resins were carefully pipetted in the countermolds, which was next covered by a glass slide and exposed to 405 nm UV light (15 s at 2 mW/cm^2) on each side, except for the R11, Formlabs Black, and Flex (30 s at 5 mW/cm^2). Test molds were removed from the countermolds and exposed to UV on each side (30 s at 5 mW/cm^2). Minimal UV doses were employed to limit the interference between casting and post-curing, while supporting successful casting. Cast molds were treated and analyzed using aforementioned protocols.

Mass Loss of the Treated Resins. Tiles of 7.5 × 7.5 × 0.75 mm^3 were cast for every resin in PDMS molds, post-cured (2 h at 14 mW/cm^2), then heated 4 h at 120 °C, and weighted between each step using a high-precision balance (AS60, Radwag, Radom, Poland) (three tiles per condition).

Sample Preparation for Spectroscopic Analysis. Similar tiles were cast with the industrial red, clear, GL4000 and PIC100 resins and treated using corresponding optimal protocols (see Table 1; UV and thermal treatment at 120 °C for the industrial red and PIC100, only UV for GL4000 and only curing at 120 °C for clear resin).

100 μL of phenylbis(2,4,6-trimethylbenzoyl)-phosphine oxide (BAPO, Sigma-Aldrich, Saint-Louis, USA) and 100 mg of ethyl(2,4,6-trimethylbenzoyl)phenyl phosphinate (TPO-L, IGM resins, Waalwijk, The Netherlands) were treated with UV (1 h at 14 mW/cm^2) followed by 2 h at 120 °C on a hotplate covered with a glass dish. Liquids (or gels) condensed on the glass dishes were collected after treatment for analysis.

https://doi.org/10.1021/acs.analchem.0c04944
Anal. Chem. 2021, 93, 7180−7187

Raman Spectroscopy. A custom-built Raman upright microscope with an excitation source (Kr + laser Innova 90-K, Coherent Inc., Santa Clara, USA; wavelength 647 nm; power 35 mW) was used for the characterization of the liquid resins; corresponding untreated and treated tiles; corresponding condensed liquids; BAPO and TPO-L untreated, treated with only UV, only heat or both UV then heat; their condensed liquids; methyl methacrylate; and (1,6)-hexanediol di-methacrylate (Sigma-Aldrich). The excitation beam was focused onto the tiles, about 5 to 70 μm below the surface. The liquid samples (40 μL) were placed in a cavity in a borosilicate glass slide. Scattered photons were collected for 100 ms and focused on a 15 μm pinhole at the entrance of a custom-made spectrograph, dispersing them in the range of −40 till +3655 rel·cm^{-1}. Spectral data were recorded with an EMCCD camera (Newton DU-970N-BV, Andor Technology Ltd., Belfast, Northern Ireland), with an average spectral resolution of 2.3 cm^{-1}. By applying a raster scan pattern covering a 30 × 30 μm^2 area, 3600 spectra were recorded for each sample. Baseline correction was applied for the treated industrial red and GL4000 resins that gave rise to significant autofluorescence.

Mass Spectroscopy Analysis. Fourier-transform ion cyclotron resonance mass spectra were acquired in a positive ion mode on a SolariX XR instrument with a 9.4 T actively shielded superconducting magnet and a dynamically harmonized cell (Bruker Daltonics, Bremen, Germany) fitted with a nano-electrospray online source. Samples (1 mg/mL in acetone) were introduced in the MS using a syringe pump (Cole-Parmer, USA) at a rate of 10 μL/min, connected to a capillary line (100 μm i.d., 360 μm o.d.), equipped with a SilicaTip needle (10 ± 1 μm, PicoTip Emitter, New Objective, USA), to which a potential of 1.3 kV was applied. The front and back trapping potentials were set at 1.6 V with a skimmer voltage at 10 V, and the ions were accumulated in the hexapole for 0.01 s. Spectra were acquired using broadband detection, 16 M data points, 150 scans accumulation, and a mass range of m/z 144 to 2000.

The instrument was calibrated using sodium trifluoroacetate (0.01 mg/mL in H_2O/MeOH 50/50 v/v) with a linear calibration. Spectra were internally calibrated in the Data Analysis software v.5.0 (Bruker Daltonics, Germany) using a list of assigned signals.

Nuclear Magnetic Resonance. NMR spectra were recorded on an AVANCE 500 (Bruker Biospin, France) operating at 202.45 MHz (^{31}P) equipped with a 5 mm triple resonance probe (TXI) at 295 K. ^{31}P spectra were acquired with proton decoupling and reported using indirect referencing. NMR chemical shifts were calibrated using residual solvent ($CDCl_3$, 7.27 ppm). All experiments were run using a software from the Bruker library, and data were processed with Topspin 4.0.

Chemical Inhibition of PDMS. A 10:1 w/w base/curing agent PDMS mixture was supplemented with chemicals or mixtures thereof, all of them at 1% w/v: pure and treated BAPO, pure and treated TPO-L, 2-benzyl-2-dimethylamino-1-(4-morpholinophenyl)-butanone-1 (Irgacure 369), 1-[4-(2-hydroxyethoxy)-phenyl]-2-hydroxy-2-methyl-1-propane-1-one (Irgacure 2959), methyl methacrylate (all Sigma-Aldrich), deep black resin, and condensed liquids/gels collected after thermal treatment of either deep black molds, or BAPO and TPO-L. These mixtures were cast on treated 3D-printed deep black molds, and test structures were imaged to quantify curing inhibition.

RESULTS AND DISCUSSION

Qualitative and Quantitative Evaluation of PDMS Curing Inhibition. First, 3D-printed test molds in the industrial red resin were employed to evaluate the PDMS curing inhibition and the effects of post-treatments. Without any post-treatment, PDMS on the mold was completely uncured (Figure 2a, right). After 1 h baking at 120 °C, the replication of sharp vertical steps (Figure 2a, center and Figure 2c, right) failed due to either incomplete curing of PDMS or its strong attachment to the mold. After 1 h UV exposure and 1 h thermal treatment at 120 °C, both the shuriken and comb test structures were perfectly replicated (Figures 2a, left and 2c, left). In an attempt to quantify PDMS curing inhibition, the "*apparent step width*" was measured, as detailed in the Experimental Section.

The apparent step width typically increased with the degree of inhibition. In a perfectly replicated structure, the wall is vertical, so that only its shadow could affect the measurement (Figure 2a, left), leading to an apparent step width <50 μm. The same illumination parameters were kept for all experiments, not to introduce any bias. Partial PDMS curing typically resulted in a damaged PDMS surface after demolding and an increased apparent width (Figure 2a, middle). In the case of severe inhibition, no step could be defined (Figure 2a, right).

Determining an Optimal Post-Treatment Recipe for 16 SLA Resins. Next, we systematically applied this methodology to 16 commercial resins from four manufacturers, exhibiting a wide range of properties (e.g., transparent, flexible, or high resolution) and therefore diverse formulations (Table 1). However, resins from DWS and Formlabs could not be processed with our printer because they strongly adhere to its Teflon-coated tank. Moreover, all resins have differences in penetration depth for the UV light, minimum dose to initiate the polymerization, or horizontal migration of activated species, which all affect the produced features and their sizes. Therefore, the resins were cast against a PDMS countermold to yield identical structures for all resins (Figure 1). All molds were subjected to the same combinations of UV exposure and baking at 60 or 120 °C. The apparent step width and thinnest properly replicated tooth were systematically determined to identify treatment recipes (Figure 2d and Tables S2 and S3). For every resin, a first recipe was defined for an "apparent step width" smaller than 50 μm and successful replication of the finest tooth (aspect ratio 2.1). This recipe typically includes baking at 120 °C, sometimes after a UV step (for 9/16 resins) with a total treatment duration shorter than 135 min for 10 resins (recipe 1, Table 1). For most of the resins (11/16), a second recipe was defined with only UV or baking at 60 °C, or a combination of both (recipe 2, Table 1). Formlabs resins and those sold as biocompatible (E-shell 300 and DS3000) were the easiest to treat. A short baking step at 120 °C (<2 h) or longer at 60 °C was sufficient, which, importantly, does not require any specialized equipment.

It is worth noticing that treatments recommended by manufacturers to complete the polymerization of the resins after 3D printing are shorter that the treatments established in this study to avoid PDMS curing inhibition (see Table S4 for an overview); yet, those "commercial" treatments are not sufficient to prevent PDMS curing inhibition. Flexible resins (flex and GL4000) were successfully treated using only UV exposure. All these recipes, established using cast molds, were next verified on 3D-printed molds for the industrial and deep black resins: for triplicate structures, an apparent step width <45 μm was found

https://doi.org/10.1021/acs.analchem.0c04944
Anal. Chem. 2021, 93, 7180−7187

and the finest tooth was successfully replicated, confirming the results obtained using cast structures.

All treatment processes were found to work for our two test structures. However, other elements should be considered for other types of structures. In our hands, higher aspect-ratio structures typically required longer UV exposures due to shadowing effects.[18,19] Some resins, when exposed to long UV exposure or high-temperature treatments (120 °C), tend to bend and change colors, and molds produced in flexible resins became harder. In the latter case, recipes using a longer thermal treatment at a lower temperature should be preferred.

Decrease in the Mold Mass after Post-Treatment. In a first hypothesis, inhibitory compounds could be eliminated through heating, which was tested by weighing tiles before and after treatment (i.e., 2 h UV exposure, followed by 4 h at 120 °C). All tiles lost mass after treatment (Figure 3), with

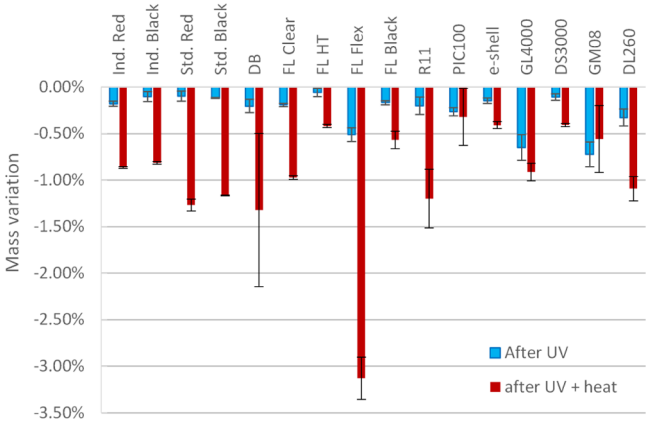

Figure 3. Variation in mass of tiles cast from 16 commercially available SLA resins, after 2 h of UV post-curing at 405 nm (blue), or a combined UV post-curing and 4 h post-baking at 120 °C (red), expressed as % of the initial mass (n = 3).

variations ranging from −0.41 ± 0.02% (DS3000) to −3.13 ± 0.23% (flex). These mass changes could be explained by the release of volatile compounds from the 3D-printed materials, which is confirmed by the condensation of liquids. This loss of mass was associated with negligible shrinkage of less than 2% (see Figure S1).

Raman Spectroscopy of Resins and Condensed Liquids. To identify potential chemical changes induced by the mold post-treatments, Raman spectroscopy analysis was performed on PIC100, clear, industrial red and GL4000 samples (liquid resins, and cast and treated molds). The inherent complexity of the resins precludes a thorough molecular analysis, and only a few major differences were found between samples (indicated by arrows on Figure 4; see Table S5 for a detailed overview). Characteristic bands of methyl methacrylate (3100, 1630, and 1400 rel·cm^{-1}, blue arrows) and hexanediol dimethacrylate monomers (Figure S2) were not found any more after casting and treatment. No significant chemical changes, unless linked to the polymerization, were identified after the post-treatment. The condensed liquids collected for PIC100, clear and industrial red were similarly analyzed. The resulting spectra for PIC100 and clear significantly differed from those of the liquid resins and acrylate monomers, suggesting that the released compounds were not highly abundant in the resins. Similar bands were detected for the industrial red condensed

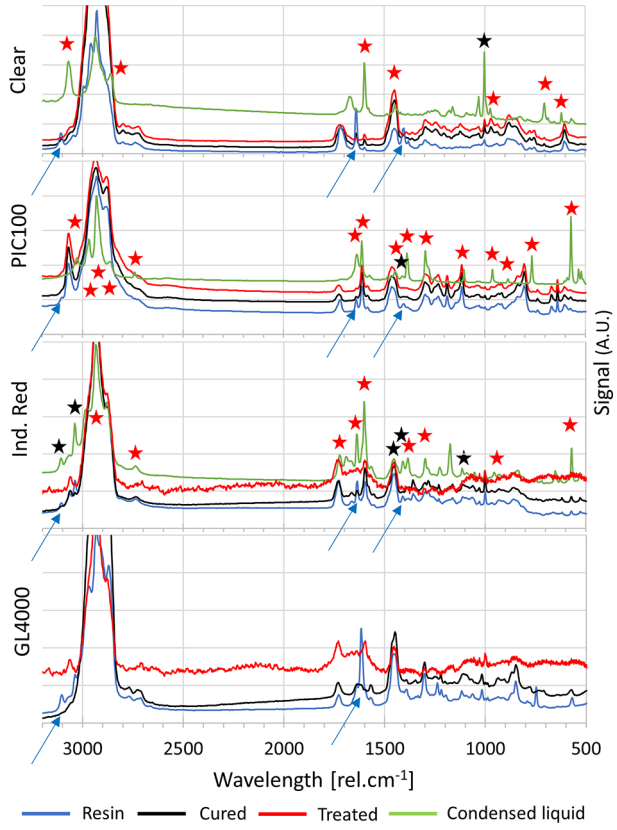

Figure 4. Raman spectra acquired for four resins (clear, PIC100, Industrial Red and GL4000) before casting (blue), after casting (black), after post-treatment (red), and for the corresponding condensed liquids (green). Arrows indicate bands being attributed to the methacrylate monomers that are not present after polymerization. Stars indicate bands found, respectively, in the BAPO and TPO-L spectra (red), and the methyl methacrylate spectrum (black).

liquid and the methacrylate monomers (black stars in Figure 4; see Table S5 for an overview).

Raman Spectroscopy Analysis of Photo-Initiators. We next examined if the condensed liquids obtained from the resins would contain photo-initiators and/or fragments thereof. Two phosphine oxide photo-initiators found in the SLA resins (BAPO and TPO-L) were subjected to several post-treatments: 1 h UV exposure, 2 h at 120 °C or combination thereof, that all yielded a similar brownish paste. BAPO (powder) lost 48.0 ± 0.2% of its mass after treatment, against 16.1 ± 5% for TPO-L (liquid).

Raman analysis of these two photo-initiators after full treatment yielded very similar spectra (Figure S2), which suggests that the post-treatment produces similar fragments for BAPO and TPO-L. Furthermore, a large number of bands detected on the Raman spectra of the resin condensed liquids were also found on the spectra of the photo-initiator condensed liquids (7/11 bands for the clear, 14/15 bands for the PIC100, and 8/15 bands for the industrial red resin, red stars in Figure 4; see Table S5 for an overview). Altogether, these data collectively suggest that the mixtures released from the 3D-printed molds through heating are very likely to contain phosphine oxide-based photo-initiators and/or fragments thereof with yet a small amount of uncured methacrylate monomers.

PDMS Curing Inhibition by Photo-Initiators and Fragments Thereof. To test if PDMS curing was inhibited by the photo-initiators, fragments thereof, and/or methacrylate

https://doi.org/10.1021/acs.analchem.0c04944
Anal. Chem. 2021, 93, 7180−7187

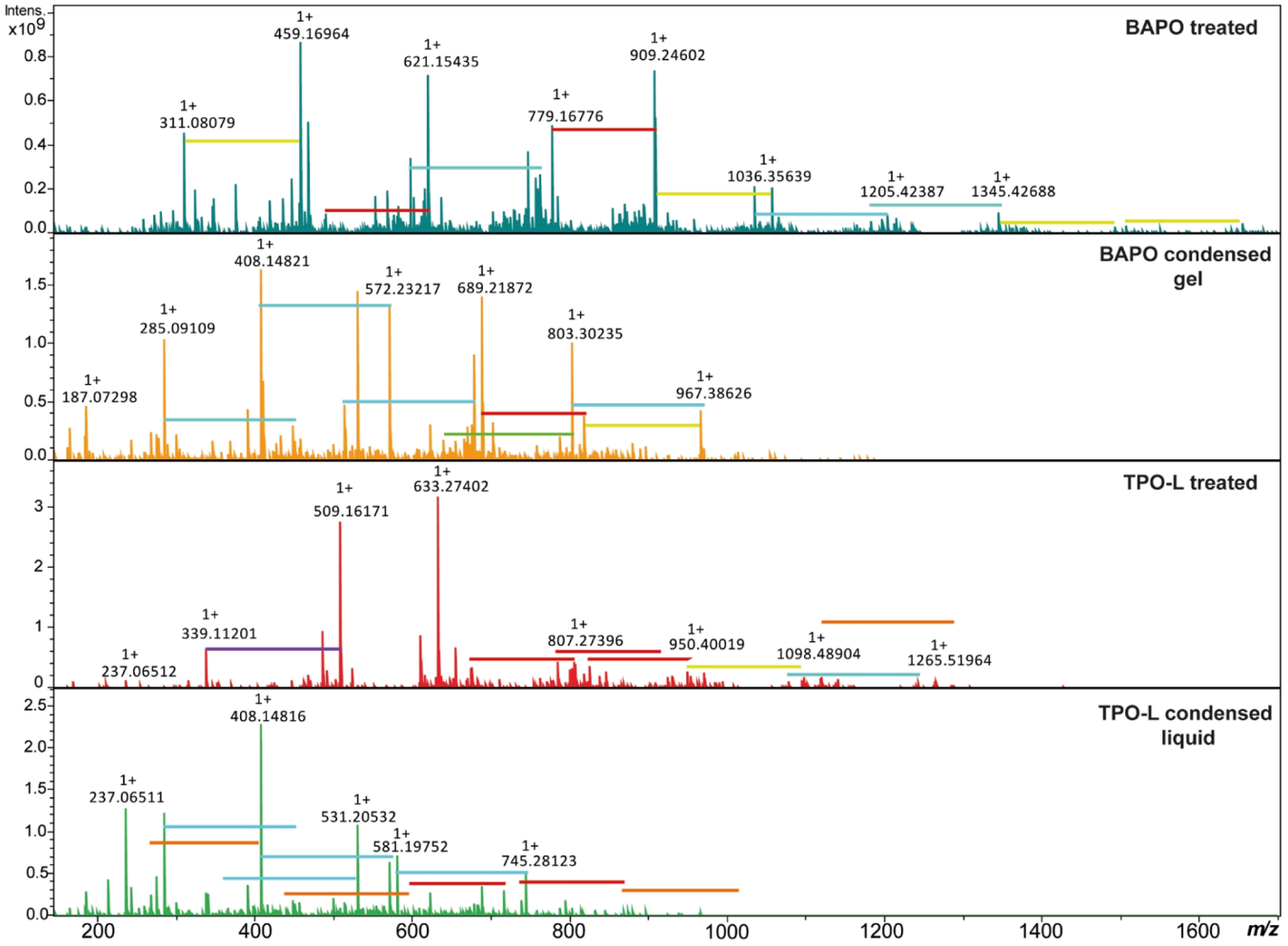

Figure 5. HR-mass spectra of BAPO and TPO-L after 1 h UV exposure and 2 h at 120 °C and of their condensed liquid collected after heat treatment. Colored horizontal lines indicate the addition of: $C_{10}H_{10}$ (m/z 130.0777, red), $C_{10}H_{10}O$ (m/z 146.0726, orange), $C_{10}H_{12}O$ (m/z 148.0882, yellow), $C_{10}H_{10}O_2$ (m/z 162.0675, green), $C_{10}H_{12}O_2$ (m/z 164.0831, blue), and $C_8H_{11}O_2P$ (m/z 170.0491, purple).

monomers, PDMS (10:1 w/w pre-polymer: curing agent) was supplemented with these compounds or one resin (deep black), its condensed liquid, and Irgacure 2959 and 369, two α-ketone photo-initiators (all at 1% w/v). These different mixtures were cured (3 h at 60 °C) on a treated test mold. FTD deep black resin and its condensed liquid strongly inhibited PDMS curing, leading to a viscous silicone paste (Figure S3), indicating that both samples contained a catalyst poison. In contrast, PDMS cured correctly in the presence of methyl methacrylate, while strongly attaching to the mold, most probably through cross-linking with the 3D-printed mold. This result is actually reminiscent of the previous work in which polyacrylate is employed to enhance adhesion between silicone-based and acrylic resin structures, while no mechanisms explaining the underlying chemistry have been proposed so far.[28] Both TPO-L and BAPO strongly inhibited PDMS curing, even after either UV or thermal treatment at 120 °C. However, after exposure to a combined treatment, these two photo-initiators formed a paste that did not solubilize anymore in PDMS, so that only a thin layer of PDMS around the paste remained uncured, while the bulk successfully polymerized. PDMS did not cure at all after supplementation with BAPO or TPO-L condensed liquids. Irgacure 2959 and Irgacure 369 which do not contain phosphorus did not inhibit PDMS curing, even at a much higher concentration (10% w/v) (data not shown). These qualitative results (Figure S3) collectively reveal that phosphine oxide-based photo-initiators are likely poisoning the PDMS catalyst, while unreacted methacrylate monomers leaching from untreated molds promote adhesion of the PDMS replica, as previously reported.[12,16,17] After a photo-thermal treatment, neither BAPO nor TPO-L did inhibit PDMS curing, in sharp contrast to their condensed liquids.

MS and NMR Analyses of Photo-Initiators. NMR and MS analyses were performed for the BAPO and TPO-L photo-initiators after a combined UV and thermal treatment, as well as on their condensed liquids to elucidate the effect of the post-treatment. ^{31}P NMR spectra (Figure S4) confirmed the presence of phosphorus on all these samples, with compounds belonging to at least two P^V families as phosphine oxide and phosphonate, and the absence of P^{III} compounds such as phosphines.[29] MS analysis demonstrated that for both photo-initiators, the treated brown pastes and the condensed liquids were composed of a large variety of molecules containing mesitoyl, phenyl, mesitylethanone, and similar groups attached to one or several phosphorus atoms, with molecular weights ranging from 311 to 1650 g/mol for the treated BAPO and 339 to 1250 g/mol for the treated TPO-L (Figure 5). Such recombination has recently been reported after photolysis of BAPO;[30] in this study, at least 16 molecules were identified and formation mechanisms proposed from the molecular formula determined using HR-

https://doi.org/10.1021/acs.analchem.0c04944
Anal. Chem. 2021, 93, 7180−7187

MS (see Figure S5). The detected molecular weights were lower for both condensed liquids compared to their treated counterparts (from m/z 187−967 for BAPO and m/z 237−795 for TPO-L). Next to this, no striking differences in chemical structures were observed.

MS analysis therefore suggests that the applied treatment induces the formation of inert high molecular weight molecules from the photo-initiators and the elimination by vaporization of low molecular weight inhibiting compounds (as the condensed liquids still inhibit PDMS curing). While this result was only obtained for two typical photo-initiators and not for the complex matrix as found in commercial resins, we can nevertheless elaborate on possible PDMS curing inhibition mechanisms. Photo-initiators in excess and their fragments produced during 3D-printing can leach from the mold into the PDMS, inhibiting its curing. During treatment, these fragments partly recombine into larger species, which are trapped in the surrounding polyacrylic network, while smaller and volatile molecules are released from the mold, both processes reducing drastically the quantity of inhibitors able to diffuse out of the molds during PDMS casting.

CONCLUSIONS

We first established a series of post-treatment, combining UV exposure and heat, using 3D-printed test structures produced from 16 SLA resins for their faithful replication in PDMS with no curing inhibition. For at least 11 of those resins, this treatment was shorter than 135 min. We believe that both the simple equipment required for these treatments and the large spectrum of resins tested in this study (resins with different properties and formulations from four manufacturers) will widely support the use of SLA for producing molds for soft lithography. We next explored the mechanisms responsible for PDMS curing inhibition to notably understand how the post-treatment could prevent this inhibition. Leaching phosphine oxide-based photo-initiator fragments were identified as PDMS catalyst poisons, while unreacted monomers would promote PDMS adhesion onto the 3D-printed molds through cross-linking reactions during PDMS curing. UV post-curing alone further polymerizes the resin, thereby limiting the risk of leaching monomers without yet avoiding the curing inhibition. Combining it with thermal treatment, on the one hand, allows for vaporizing the remaining photo-initiators out of the 3D-printed structures and, on the other hand, promotes recombination reactions between the photo-initiator fragments to yield high MW species that remain trapped in the 3D-printed resin. This mechanism is likely to be valid for resins using phosphine-oxide based photo-initiators and silicone polymers such as PDMS using a Pt-based catalyst, as is the case for Sylgard 184 and RTV 615.[12] Reducing leaching from 3D-printed objects has already been reported to also improve their biocompatibility and the survival of cells cultured in their direct vicinity.[31] While this would require additional studies, our generic treatment is also likely to significantly improve the biocompatibility of resins and support their use to produce organ-on-a-chip models, directly using 3D printing.

ASSOCIATED CONTENT

Supporting Information

The Supporting Information is available free of charge at https://pubs.acs.org/doi/10.1021/acs.analchem.0c04944.

Overview of previously reported post-treatments to suppress PDMS curing inhibition on 3D-printed molds; post-treatment screenings for protocols including UV exposure and heating at 120 °C and 60 °C, respectively; comparison between post-treatments recommended by Formlabs and those proposed in this study; influence of the post-treatment on the dimensions of 3D printed structures; overview of the bands in the Raman spectra—comparison between spectra; Raman spectra of monomers and BAPO and TPO-L; pictures of PDMS supplemented with various resins, condensed liquids thereof, photo-initiators and condensed liquids thereof, or monomers after casting; ^{31}P NMR spectra for BAPO and TPO-L; and identification of compounds from the MS analysis of the treated BAPO and TPO-L and possible formation mechanisms (PDF)

AUTHOR INFORMATION

Corresponding Authors

Bastien Venzac − *Applied Microfluidics for BioEngineering Research, MESA+ Institute for Nanotechnology & TechMed Centre, University of Twente, 7500AE Enschede, The Netherlands*; Email: bastien.venzac@laas.fr

Séverine Le Gac − *Applied Microfluidics for BioEngineering Research, MESA+ Institute for Nanotechnology & TechMed Centre, University of Twente, 7500AE Enschede, The Netherlands*; orcid.org/0000-0002-4546-6184; Email: s.legac@utwente.nl

Authors

Shanliang Deng − *Applied Microfluidics for BioEngineering Research, MESA+ Institute for Nanotechnology & TechMed Centre, University of Twente, 7500AE Enschede, The Netherlands*

Ziad Mahmoud − *Université Lille, CNRS, USR 3290, MSAP, Miniaturisation pour la Synthèse l'Analyse et la Protéomique, 59000 Lille, France*; orcid.org/0000-0002-5563-0558

Aufried Lenferink − *Medical Cell BioPhysics, TechMed Centre, University of Twente, 7500AE Enschede, The Netherlands*

Aurélie Costa − *Université Lille, CNRS, USR 3290, MSAP, Miniaturisation pour la Synthèse l'Analyse et la Protéomique, 59000 Lille, France*

Fabrice Bray − *Université Lille, CNRS, USR 3290, MSAP, Miniaturisation pour la Synthèse l'Analyse et la Protéomique, 59000 Lille, France*

Cees Otto − *Medical Cell BioPhysics, TechMed Centre, University of Twente, 7500AE Enschede, The Netherlands*

Christian Rolando − *Université Lille, CNRS, USR 3290, MSAP, Miniaturisation pour la Synthèse l'Analyse et la Protéomique, 59000 Lille, France; Shrieking Sixties, 59650 Villeneuve-d'Ascq, France*; orcid.org/0000-0002-3266-8860

Complete contact information is available at: https://pubs.acs.org/10.1021/acs.analchem.0c04944

Author Contributions

B.V. designed the study, conducted part of the experiments analyzed data, and wrote the manuscript; S.D. conducted experiments on the post-treatment identification for resins and to evaluate mass loss after post-treatment; Z.M. and F.B. conducted MS analysis, analyzed spectra and, together with A.C., identified chemical species and proposed recombination

https://doi.org/10.1021/acs.analchem.0c04944
Anal. Chem. 2021, 93, 7180−7187

mechanisms; C.R. supervised MS and NMR analysis; A.L. conducted Raman spectroscopy analysis with B.V.; C.O. supervised Raman spectroscopy analysis; S.L.G. designed the study and wrote the manuscript; all authors commented on the manuscript and approved of its content.

Notes

The authors declare no competing financial interest.

■ ACKNOWLEDGMENTS

The authors thank Prof. Nathalie Azaroual and Alexandre Rech from the GRITA laboratory for recording NMR spectra. The NMR and Mass Spectrometry facilities are funded by the European Regional Development Fund, Région Haut-de-France (France), the CNRS, and the University of Lille. Access to the FT-ICR MS in the frame of the EU_FT-ICR_MS network installation is funded by the EU Horizon 2020 grant 731077; support for conducting research is gratefully acknowledged.

■ REFERENCES

(1) Duffy, D. C.; Mcdonald, J. C.; Schueller, O. J. A.; Whitesides, G. M. *Anal. Chem.* **1998**, *70*, 4974−4984.
(2) Delamarche, E.; et al. *Science* **1997**, *276*, 779−781.
(3) M, K. R.; Chakraborty, S. *J. Appl. Polym. Sci.* **2020**, *137*, 48958.
(4) Yousuff, C.; Danish, M.; Ho, E.; Kamal Basha, I.; Hamid, N. *Micromachines* **2017**, *8*, 258.
(5) Kaigala, G. V.; Ho, S.; Penterman, R.; Backhouse, C. J. *Lab Chip* **2007**, *7*, 384.
(6) Branham, M. L.; Tran-Son-Tay, R.; Schoonover, C.; Davis, P. S.; Allen, S. D.; Shyy, W. *J. Mater. Res.* **2002**, *17*, 1559−1562.
(7) Mcdonald, J. C.; Chabinyc, M. L.; Metallo, S. J.; Anderson, J. R.; Stroock, A. D.; Whitesides, G. M. *Anal. Chem.* **2002**, *74*, 1537−1545.
(8) Glick, C.; et al. *Microsyst. Nanoeng.* **2016**, *2*, 16063.
(9) Balakrishnan, H. K.; Badar, F.; Doeven, E. H.; Novak, J. I.; Merenda, A.; Dumée, L. F.; Loy, J.; Guijt, R. M. *Anal. Chem.* **2021**, *93*, 350−366.
(10) Accardo, A.; Courson, R.; Riesco, R.; Raimbault, V.; Malaquin, L. *Addit. Manuf.* **2018**, *22*, 440−446.
(11) Comina, G.; Suska, A.; Filippini, D.; German Comina, A. S.; Filippini, D. *Lab Chip* **2014**, *14*, 424−430.
(12) Chan, H. N.; Chen, Y.; Shu, Y.; Chen, Y.; Tian, Q.; Wu, H. *Microfluid. Nanofluid.* **2015**, *19*, 9−18.
(13) Costa, P. F.; et al. *Lab Chip* **2017**, *17*, 2785−2792.
(14) Dinh, T.; Phan, H.-P.; Kashaninejad, N.; Nguyen, T.-K.; Dao, D. V.; Nguyen, N.-T. *Adv. Mater. Interfaces* **2018**, *5*, 1800764.
(15) Razavi Bazaz, S.; Kashaninejad, N.; Azadi, S.; Patel, K.; Asadnia, M.; Jin, D.; Ebrahimi Warkiani, M. *Adv. Mater. Technol.* **2019**, *4*, 1900425.
(16) Waheed, S.; et al. *Sci. Rep.* **2017**, *7*, 15109.
(17) King, P. H.; Jones, G.; Morgan, H.; de Planque, M. R. R.; Zauner, K.-P. *Lab Chip* **2014**, *14*, 722−729.
(18) Ferraz, M. d. A. M. M.; Nagashima, J. B.; Venzac, B.; Le Gac, S.; Songsasen, N. *Sci. Rep.* **2020**, *10*, 994.
(19) Ferraz, M. d. A. M. M.; Nagashima, J. B.; Venzac, B.; Le Gac, S.; Songsasen, N. *Sci. Rep.* **2020**, *10*, 1575.
(20) Olanrewaju, A. O.; Robillard, A.; Dagher, M.; Juncker, D. *Lab Chip* **2016**, *16*, 3804−3814.
(21) Flowers, G. L.; Switzer, S. T. *Background Material Properties of Selected Silicone Potting Compounds and Raw Materials for Their Substitutes; MHSMP-78-18*; Mason and Hanger-Silas Mason Co., Inc.: Amarillo, Tex. (USA), 1978.
(22) Faglioni, F.; Blanco, M.; Goddard, W. A.; Saunders, D. *J. Phys. Chem. B* **2002**, *106*, 1714−1721.
(23) Kownacki, I.; et al. *Appl. Catal., A* **2009**, *362*, 106−114.
(24) Lewis, L. N.; Stein, J.; Colborn, R. E.; Gao, Y.; Dong, J. *J. Organomet. Chem.* **1996**, *521*, 221−227.
(25) de Almeida Monteiro Melo Ferraz, M.; et al. *Environ. Sci. Technol. Lett.* **2018**, *5*, 80−85.
(26) Oskui, S. M.; Diamante, G.; Liao, C.; Shi, W.; Gan, J.; Schlenk, D.; Grover, W. H. *Environ. Sci. Technol. Lett.* **2016**, *3*, 1−6.
(27) Carve, M.; Wlodkowic, D. *Micromachines* **2018**, *9*, 91.
(28) Chang, P. P.; Hansen, N. A.; Phoenix, R. D.; Schneid, T. R. *J. Prosthodont.* **2009**, *18*, 23−31.
(29) Kolczak, U.; Rist, G.; Dietliker, K.; Wirz, J. *J. Am. Chem. Soc.* **1996**, *118*, 6477−6489.
(30) Schmallegger, M.; et al. *Chem.—Eur J.* **2019**, *25*, 8982−8986.
(31) Piironen, K.; Haapala, M.; Talman, V.; Järvinen, P.; Sikanen, T. *Lab Chip* **2020**, *20*, 2372−2382.

https://doi.org/10.1021/acs.analchem.0c04944
Anal. Chem. 2021, 93, 7180−7187